IEEE Access
Multidisciplinary ⋮ Rapid Review ⋮ Open Access Journal

Received December 24, 2019, accepted February 27, 2020, date of publication March 5, 2020, date of current version March 17, 2020.

Digital Object Identifier 10.1109/ACCESS.2020.2978391

Wearable Multi-Biosignal Analysis Integrated Interface With Direct Sleep-Stage Classification

SUNG-WOO KIM[1], KWANGMUK LEE[1], JUNYEONG YEOM[1], TAE-HOON LEE[2], DON-HAN KIM[3], AND JAE JOON KIM[1], (Senior Member, IEEE)

[1]School of Electrical and Computer Engineering, Ulsan National Institute of Science and Technology (UNIST), Ulsan 44919, South Korea
[2]Department of Otolaryngology-Head and Neck Surgery, Ulsan University Hospital, Ulsan 44033, South Korea
[3]Department of Digital Contents, University of Ulsan, Ulsan 44610, South Korea

Corresponding author: Jae Joon Kim (jaejoon@unist.ac.kr)

This work was supported in part by the Institute of Information and Communications Technology Planning and Evaluation (IITP) grant funded by the Ministry of Science and ICT, South Korea (Development of Disposable IoT Nanosensors for Environmental Monitoring and Biosignal Detection and Development of Unconscious Real-Time Stress/Blood Pressure Wearable System for Work-Stress Monitoring and Management), under Grant 2018-0-00756 and Grant 2019-0-00208, in part by the Samsung Electronics, and in part by the National Research Foundation of Korea under Grant 2017M1A2A2087833.

ABSTRACT This paper presents a wearable multi-biosignal wireless interface for sleep analysis. It enables comfortable sleep monitoring with direct sleep-stage classification capability while conventional analytic interfaces including the Polysomnography (PSG) require complex post-processing analyses based on heavy raw data, need expert supervision for measurements, or do not provide comfortable fit for long-time wearing. The proposed multi-biosignal interface consists of electroencephalography (EEG), electromyography (EMG), and electrooculography (EOG). A readout integrated circuit (ROIC) is designed to collect three kinds of bio-potential signals through four internal readout channels, where their analog feature extraction circuits are included together to provide sleep-stage classification directly. The designed multi-biosignal sensing ROIC is fabricated in a 180-nm complementary metal–oxide–semiconductor (CMOS) process. For system-level verification, its low-power headband-style analytic device is implemented for wearable sleep monitoring, where the direct sleep-stage classification is performed based on a decision tree algorithm. It is functionally verified by comparison experiments with post-processing analysis results from the OpenBCI module, whose sleep-stage detection shows reasonable correlation of 74% for four sleep stages.

INDEX TERMS Sleep-stage classification, multi-biosignal interface, rule-based decision tree, feature extraction stage, readout integrated circuit, wearable device.

I. INTRODUCTION

Sleep is a kind of indispensable metabolic activity that energizes the human body and boosts its immunity, and sleep disorders can cause illness in the body as well as degradation of physical conditions [1]. They typically include rapid eye movement (REM) sleep behavior disorder, nocturnal enuresis, sleepwalking, etc., which may cause serious injury during sleep [2]. According to a survey [3], sleep deprivation and disability occur in a significant part of the world's population, 30% of adults suffering from insomnia. Moreover, prevalence of obstructive sleep apnea is 9 to 21 %, which increases to 24 to 31 % among males. Therefore, it necessitates some methods for sleep quality monitoring, where the golden standard for this purpose is the polysomnography (PSG).

The PSG measures REM and non-REM (NREM) step characteristics during three sleep stages, whose measurement is carried out by using nine types of human body signals and electrode bundles belonging to them [4]. It can perform accurate sleep analysis and diagnosis, but its inspection process is complicated and difficult, requiring hospitalization burden with an expert to be stationed. Like this, the PSG-based sleep analysis gives uncomfortable access to treatment of sleep diseases. Therefore, there have been researches on healthcare devices for self-monitoring sleep stage or quality [5]. Their common characteristic is that they are in the form of portable device type which is easy to carry and comfortable to be measured at home [6]. Besides, they have been designed to have wireless monitoring interfaces without storing massive data

The associate editor coordinating the review of this manuscript and approving it for publication was Usama Mir.

into optical or semiconductor storage devices [7]. However, most works were limited to partial sleep analyses or simple monitoring functions based on heart rate, body movement, and so on.

Recently, sleep monitoring devices evolve to be more accurate or to provide better user-centric interfaces [8], [9], which also offers intuitive solutions with smartphones. The Sleep Profiler of the Advanced Brain Monitoring [8] provides effective PSG-compatible interfaces with reasonable accuracy. But it does not integrate its analysis function, providing an indirect solution with on-line diagnosis. The SmartSleep device of the Philips [9] provides a smartphone-based user-centric interface that allows easy sleep testing and provides a solution for sleep quality right after sleep. However, it utilizes only the single-channel electroencephalography (EEG), whose reliability is not enough in comparison with the PSG-compatible interface. Another wearable research with dry electrodes in headband [10] gives in-home sleep monitoring interface, but it does not have its own sleep analysis environment. There have been wearable device studies on detection algorithms for sleep apnea patients [11], [12], not including sleep-stage analyses. Therefore, a wearable multi-biosignal analysis integrated interface including direct sleep-stage detection is proposed in this work. Fig. 1 shows a proposed sleep monitoring process, where direct sleep-stage classification capability is provided together with conventional monitoring functions under post-processing sleep analysis environments. The conventional process has a device configuration that is carried out by person, where it serves as a recording device similar to the PSG interface configuration. This proposed work serves as a multi-biosignal sensing interface that can be selectively configured to provide the direct sleep-stage classification based on three kinds of biosignals such as EEG, electromyography (EMG), and electrooculography (EOG).

The rest of this paper is organized as follows. Section II describes the proposed multi-biosignal analysis integrated interface system. Section III presents detailed implementation of its multi-biosignal sensing readout integrated circuit (ROIC). Section IV shows experimental results, and then conclusions are drawn in Section V.

II. MULTI-BIOSIGNAL ANALYSIS INTERFACE SYSTEM

The proposed multi-biosignal analysis integrated interface has dual signal processing structure for sleep analysis as seen in Fig. 1, where it provides two processing modes of monitoring and analysis. Firstly, a multi-biosignal sensing ROIC is designed to detect multiple biopotential signals such as EEG, EMG, and EOG. After its analog front-end for amplifying and filtering, then the signal processing path is divided into the monitoring mode and the analysis mode, depending on applicational purposes. In case of the analysis mode, amplified signals go to proposed feature extraction stages. The EEG feature extraction characterizes brain waves during sleep by using the scoring manual of the American Academy of Sleep Medicine (AASM). Since its output format is digital, its digital output is delivered to the microcontroller

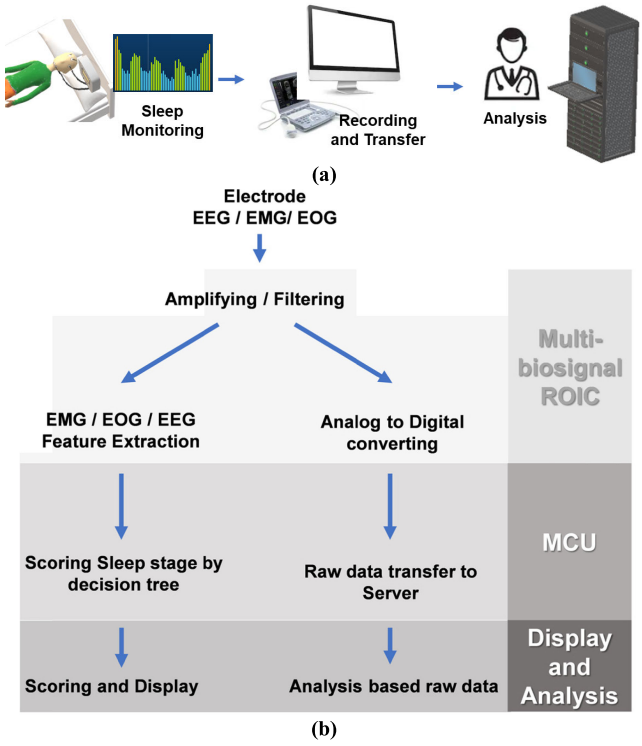

FIGURE 1. Proposed sleep analysis process embedding (a) conventional post-processing method and (b) direct sleep-stage classification method.

unit (MCU) via the serial peripheral interface (SPI). Then, a decision tree algorithm scores the sleep stage based on digital feature extraction outputs. In case of the monitoring mode, measured raw signals are directly digitized by a 16-bit sigma-delta analog-to-digital converter (ADC) in the ROIC, and then they are delivered to desktop computers or computing servers for application-specific signal processing procedures. While this monitoring mode corresponds to conventional post-processing methods, the analysis mode in the proposed dual-mode structure enables direct sleep-stage classification without additional post-processing works, where real-time sleep stages can be directly displayed.

The sleep stages generally consist of three phases: wake, NREM, and REM [4], where the NREM stage is divided further depending on applications. The AASM divides the NREM into three stages of N1, N2, and N3. During sleep, the N1 stage which corresponds to shallow sleep is within 5 % of the total sleep period, and it is measured as transition time between the wake and the N2. On the other hand, the N2 occupies about half of the total while the N3 and the REM account for 20 % to 25 % respectively. Therefore, the N1 is insignificant compared to other stages in terms of time length, and also its waveform characteristics representing the sleep period are unclear [10], [13]–[15]. Therefore, in order to improves the accuracy of sleep-stage detection, this work is designed to adopt four phases of wake (W), shallow sleep (SS), deep sleep (DS), and REM, which has been also applied to existing wearable device products such as smartwatches and

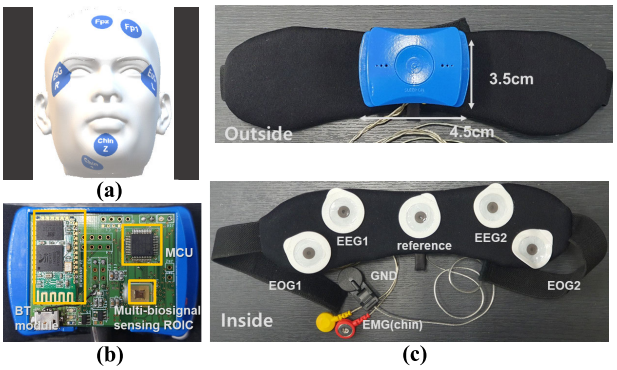

FIGURE 2. Proposed multi-biosignal interface for sleep monitoring: (a) electrode placement, (b) sensor module, and (c) Smart headband.

headbands [16]. As in [16], the N2 and the N3 correspond to the SS and the DS respectively.

The proposed analysis interface is designed to provide direct sleep-stage classification capability. Three analog feature extraction circuits on the EEG, the EMG, and the EOG are newly provided and integrated together in the ROIC. Based on these feature signals, the sleep stage is directly estimated by utilizing the decision tree algorithm [17]. Fig. 2(a) presents the electrode placement of the proposed system, whose location is based on the international 10-20 system [18]. The EEG is measured on the forehead, and the EOG and the EMG are from the eye temple and the submental respectively, where the clip-type ground electrode is attached to the earlobe. The conventional EEG probing requires three different electrode placements, but the single-channel EEG analysis has been actively studied for healthcare devices whose reliability has been recognized [19], [20]. Fig. 2(b) shows a sensor module prototype which consists of the multi-biosignal sensing ROIC, the low-power MCU (STM32L4), and the Bluetooth (BT) module (HC-06). Its BT-based monitoring interface is implemented to support wireless connections to both the smartphone and the desktop computer. The overall power consumption of the multi-biosignal analysis integrated interface is 70.9mW where the ROIC occupies 0.9mW. Fig. 2(c) presents a headband-style protype, named as 'Smart Headband', which enables convenient sleep analysis. It consists of a headband of rubber and mesh material, electrodes, and a sensor module box. The module box size is 3.5 cm × 4.5 cm, and the headband size is 3 cm × 12 cm.

III. MULTI-BIOSIGNAL SENSING ROIC

Fig. 3 presents the overall structure of the designed multi-biosignal sensing ROIC, where it is divided into two parts of the analog front-end stage and the feature extraction stage. The ROIC also includes the low-dropout regulator with the bandgap voltage reference, the SPI, the clock generator, the 16-bit sigma-delta ADC. The analog front-end stage consists of four readout channels including one EEG, two EOGs, and one EMG. When bio-potential signals are read through their module electrodes, they are amplified and filtered properly according to inherent characteristics of each biosignal. The feature extraction stage includes three kinds of feature extraction circuits for the EEG, the EMG, and the EOG, whose extraction outputs would be utilized to diagnosis or classify transient sleep stages. The feature extraction outputs for the analysis mode and the sigma-delta ADC outputs for the monitoring mode are delivered through the SPI to the MCU.

A. ANALOG FRONT END

Fig. 4 illustrates the schematic of a pre-amplification stage in the analog front end, including a low-noise amplifier (LNA) with the chopper stabilization and a switched-capacitor programmable-gain amplifier (PGA). In particular, the LNA is designed to utilize the chopper stabilization for better immunity to low-frequency noises. Also, it resolves DC offset due to mismatch by using the DC servo loop and reduces transient fluctuations by using the ripple reduction loop. These techniques reduce not only noises but also implement high-pass filtering whose cut-off frequency can be tuned

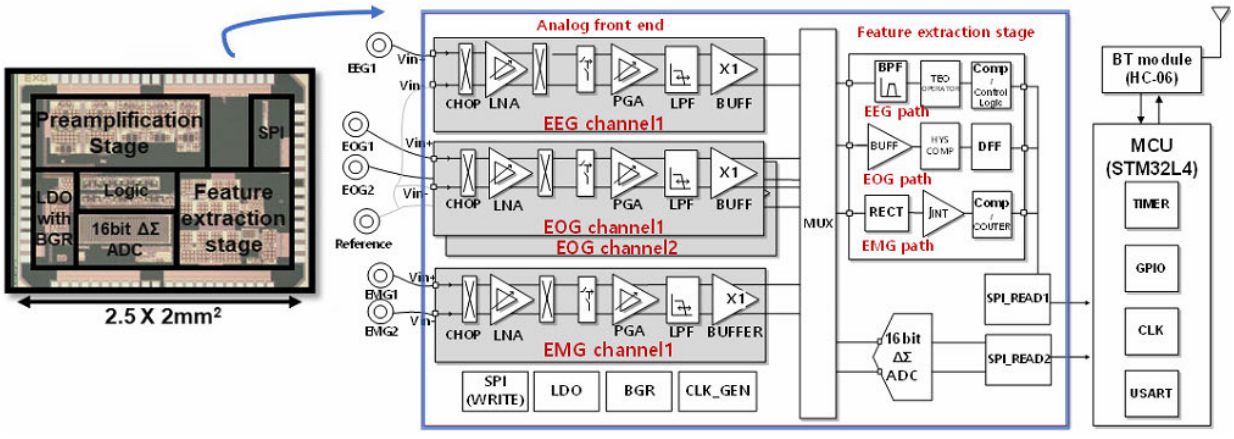

FIGURE 3. Multi-biosignal sensing readout integrated circuit (ROIC).

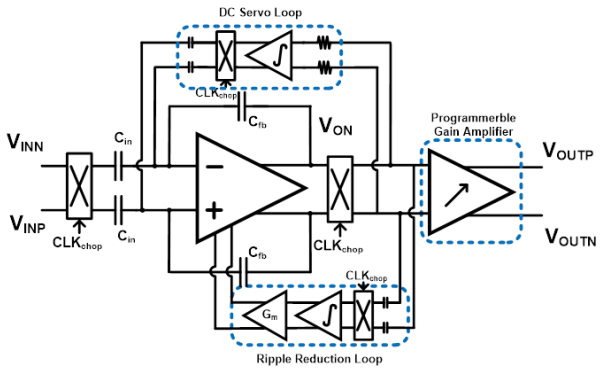

FIGURE 4. Schematic of pre-amplifier stage with low-noise amplifier (LNA) and programmable gain amplifier (PGA).

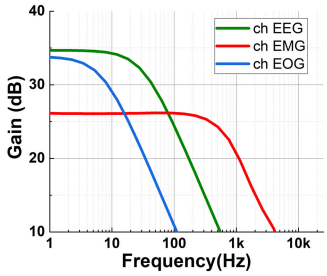

FIGURE 5. Programmable characteristics of PGA gain and bandwidth for multiple biosignals.

from 0.6 Hz to 7 Hz. The EEG frequency ranges from 4 to 30 Hz. The EOG has several Hz when waking and REM sleep, and the EMG has 300 Hz range. So, the PGA is designed to have programmable bandwidths of 30Hz, 6Hz, and 300Hz depending on biosignal kinds of EEG, EOG, and EMG. Its gain is also tuned to be 35, 33, and 26dB respectively. Fig. 5 shows frequency characteristics of the PGA for multi-biosignal channels which are utilized for sleep analysis.

B. FEASTURE EXTRACTION CIRCUITS

The feature extraction is usually performed by fast Fourier transform (FFT)-based or spectrum analyses in the frequency domain. Its detailed methods are primarily subdivided into linear discriminant analysis, artificial neural network, support vector machine, and k-nearest neighbors, which have high accuracy and reliability. However, they would be performed in computing servers or desktop computers, which is not suitable for wearable-healthcare devices [21]. Whereas, this work presents time-domain signal processing methods for sleep analyses that can be easily implemented inside wearable healthcare devices. That is, time-domain feature extraction informations are gathered from proposed analog circuits in biopotential readout channels, which are utilized for the sleep analysis based on the rule-based decision tree inside the MCU. Fig. 6 shows three kinds of feature extraction circuit for EEG, EMG, and EOG, where their behavioral descriptions are give together with characteristic time-domain waveforms. Fig. 6(a) shows the teager energy operator (TEO) as the feature extraction circuit for the EEG. First, the EEG signal after the analog front end is delivered to a band pass filter (BPF) for classification of specific sleep stage. Then, it goes through the TEO that is composed of a low-pass filter and a multiplier to measure instantaneous energy. According to [22], the TEO is designed by the following formulas of coninuous-time and discrete-time.

$$\Psi[\mathrm{x}\,(\mathrm{t})] = \left(\frac{\mathrm{dx}\,(\mathrm{t})}{\mathrm{dt}}\right)^2 - x(t)\frac{d^2x(t)}{dt^2} \tag{1}$$

$$\Psi\,[x\,(n)] = x_n^2 - x_{n+1}x_{n-1} \tag{2}$$

Equation (1) corresponds to a differential operator circuit with high-pass filter configuration. However, this is not suitable for biological signals below 30Hz, which is the frequency characteristic of EEG. Instead, if the discrete domain method in (2) is adopted, it can be implemented with low-pass filter configuration which is more suitable for the EEG signal [23], [24]. In addition, the current consumption of the TEO circuit can be reduced, since the transconductance of internal amplifiers can be reduced in case of low-frequency pole implementaion for the EEG. The BPF before the TEO is designed to have the pass band of 11 to 16 Hz, and then the EEG is filtered to have the frequency of the N2 sleep stage through the TEO circuit, which derives the sleep spindle. This instant filtered outputs are compared with its normalized or averaged value. This comparison output, which corresponds to 1-bit digital output of the TEO circuit, is utilized to distinguish between two sleep stages of SS and DS in the decision tree algorithm of the MCU.

Fig. 6(b) is a signal level detector specialized to detect the strength of the EMG waveform during sleep [25], which gives featured distinction between non-REM sleep and REM sleep. In the beginning of sleep, the EMG becomes weaker, and in the REM sleep stage, it becomes atonia with waveform amplitude less than 1 uV [26]. The signal level detector circuit consists of a rectifier circuit, an integrator, a comparator and a counter. First, the EMG input goes through the rectifier to extract its strenth or amplitude information which changes the charging speed of the following integrator. If the integrator output becomes bigger than a critical value, the comparator generates a short pulse. Then, the counter calculates the pulse interval which corresponds to the EMG strength information. In this way, the proposed EMG level detector performs the feature extraction function to distinguish non-REM or REM sleep stages.

Fig. 6(c) shows a signal peak detector circuit for the EOG feature detection. While there are no spurious peaks in the EOG waveform during non-REM sleep, the EOG waveform in the REM sleep stage shows sharp peaks with the frequency exceeding 2Hz. When this peak signal appears, two EOG waveforms from both eyes has reverse phase relationship, which is an inherent feature of the REM sleep stage. Therefore, the signal peak detector needs to be designed to detect the EOG peak pair with the reverse phase relationship. For this purpose, four buffered paths for each EOG input are

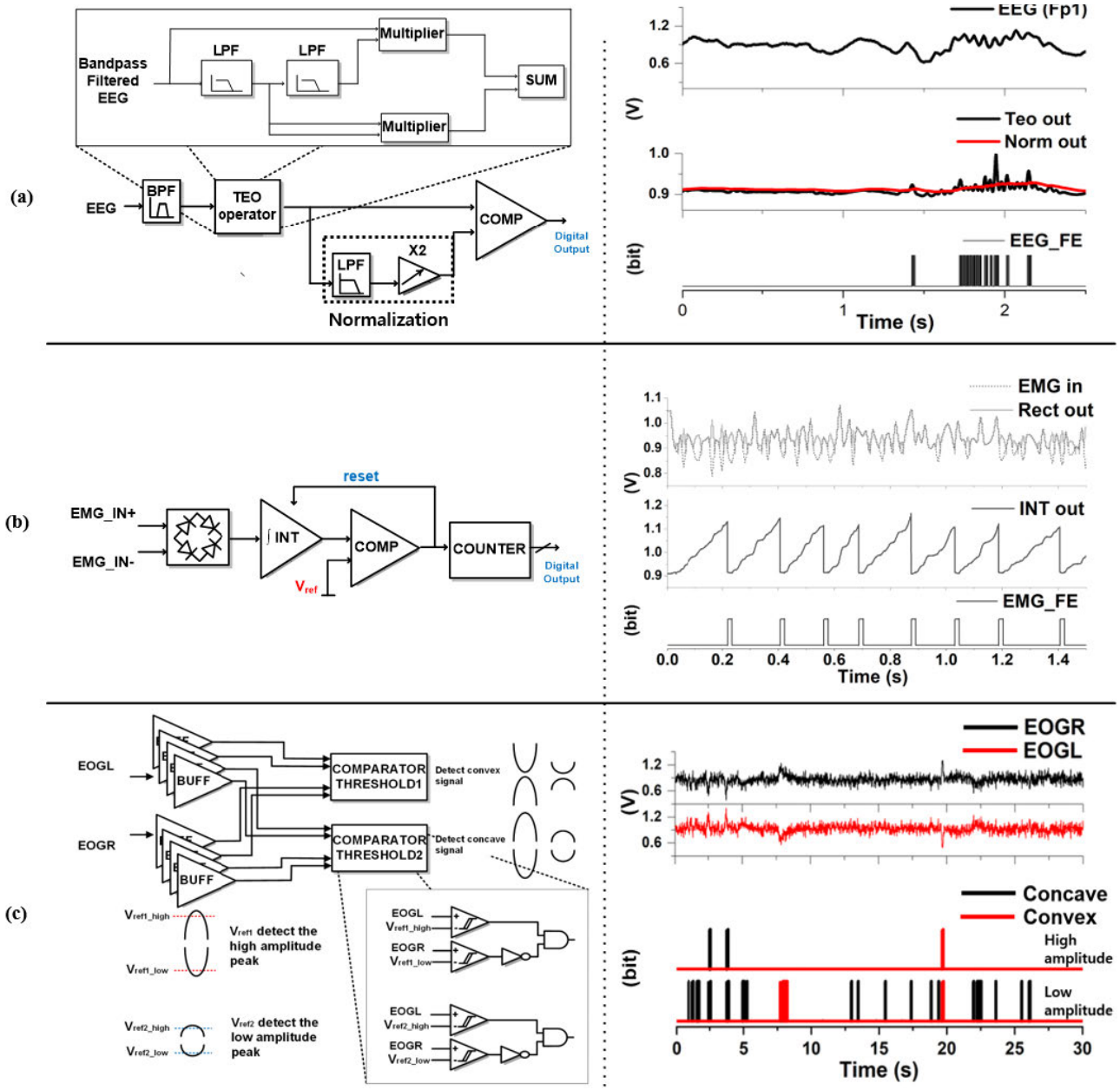

FIGURE 6. Feature extraction measurements: (a) TEO operator for EEG, (b) signal level detector for EMG, and (c) signal peak detector for EOG.

followed by two hysteresis comparators with one pair of reference voltages. Depending on target signal swing amplitude to be detected, the reference voltage pair is adjusted to give high or low amplitude detection. The right side of Fig. 6(c) shows its operational waveforms for the EOG feature extraction during the REM stage. Two upper waveforms show EOG signal waveforms from both eyes, and two lower waveforms are low/high digital comparison outpusts for the feature extraction. Interconnections between the MCU and the ROIC are shown in Fig. 7, where a 16-bit SPI interface is implemented for serial communication of data and control singals.

C. SLEEP-STAGE CLASSIFICATION

Table 1 summarizes featured characteristics of sleep stages according to the AASM. The EOG frequency shows significant difference between the wake and the REM. It is below 2 Hz due to eye blinking during the wake, but it goes over 2 Hz during the REM. In case of the SS stage, weak sinusoidal eye movement (SEM) appears. The EEG waveform slows down gradually as the stage goes from the wake to the DS. Then, when the stage enters the REM, the frequency rises slightly. The EMG strength becomes weaker as the stage goes from the wake via the SS and the DS to the REM. Based on counting these inherent features for sleep stages,

TABLE 1. Featured characteristics of sleep stages.

	Wake	Shallow Sleep (N1,N2)	Deep Sleep (N3)	REM
EOG (frequency)	0.5~2Hz Blink	SEM	-	Over 2Hz Blink
EMG (relative tone)	High	High - Medium	Small	Very small
EEG (frequency)	8~13Hz (alpha wave)	11 – 16Hz (Sleep spindle)	0.5-2Hz (delta wave)	4-7Hz (theta+alpha wave)

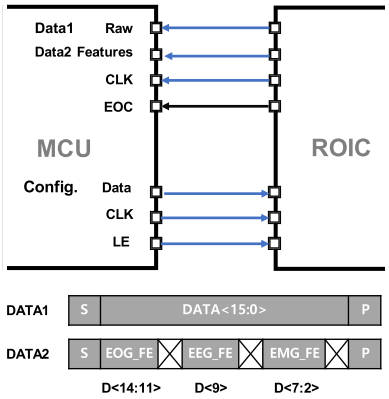

FIGURE 7. Serial data format for MCU-ROIC interface.

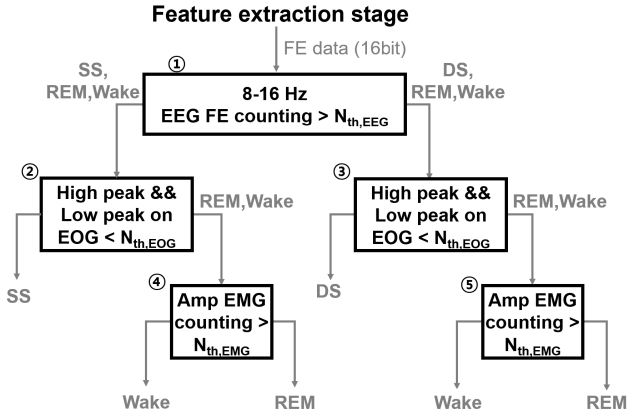

FIGURE 8. Diagram of proposed decision tree algorithm for direct sleep-stage classification.

the proposed stage classification is performed by the decision tree as shown in Fig. 8. After sleep, occurrences of the sleep spindle are counted through the EEG TEO operator, and then decision between the SS and the DS is made depending on the counted value, whose comparison threshold is empirically given. After this SS-DS classification, the next procedure is to monitor whether the stage goes to the REM or not, by utilizing the weighted counting of the EOG peak detection. Then, through the counting process of the EMG level detection, the next classification between the REM and the wake is performed. Table 2 presents detailed rules on decision tree nodes. If the rule on each decision node is satisfied through the weighted counting process for one epoch of 30-second long, the next epoch state goes to the left side.

TABLE 2. Comparison rules on decision tree nodes.

rule	comparative stages	condition
1	SS/DS	EEG FE counting > $N_{th,EEG}$
2	SS/REM,Wake	High and low peak detection on EOG < $N_{th,EOG}$
3	DS/REM,Wake	High and low peak detection on EOG < $N_{th,EOG}$
4	Wake/REM	EMG amplitude counting > $N_{th,EMG}$
5	Wake/REM	EMG amplitude counting > $N_{th,EMG}$

Otherwise, it goes to the right side. These sleep-stage classification processes including the weighted counting and the decision-tree algorithm are fully implemented on the MCU so that the sleep-stage is directly classified without additional post-processing works.

IV. MEASUREMENT RESULTS

For feasibility of the proposed multi-biosignal analysis interface with the direct sleep-stage classification capability, the headband-style wearable prototype in Fig. 2 was manufactured together with the multi-biosignal ROIC in Fig. 3. For their experimental verification, a proven dataset-based compatibility experiment and a comparison experiment with a commercial product were performed in parallel. Firstly, the proven dataset-based experiment utilized common public sleep datasets [27], especially the sleep-EDF database which contains PSG records with multi-biosignals [28]. With the sleep-EDF datasets, the proposed EEG feature detector was functionally verified to discriminate between the SS and the DS, whose experiment environments and results are shown in Fig. 9. Based on the sleep-EDF datasets in CSV file format, simulated EEG waveforms for sleep stages were generated and inserted into the proposed analysis interface module. The tablet on the left side of Fig. 9 shows real-time monitoring results from the EEG feature detector, and its upper right-hand side shows oscilloscope-probed analog waveforms from the analog front end of the ROIC, where feature extraction output waveforms differ because the EE frequency form the SS is higher than that from the DS. For performance evaluation of the proposed method to distinguish between the SS and the DS, three performance metrics of sensitivity, specificity, and accuracy are computed by the following equations:

$$\text{Sensivity} = \frac{\text{TP}}{\text{TP}+\text{FN}}$$
$$\text{Specifity} = \frac{\text{TN}}{\text{TN}+\text{FP}}$$
$$\text{Accuracy} = \frac{\text{TN}+\text{TP}}{\text{TN}+\text{TP}+\text{FN}+\text{FP}},$$

where TP is the true positive, TN is the true negative, FP is the false positive, and FN is the false negative. Measured performance metrics through the proposed multi-biosignal

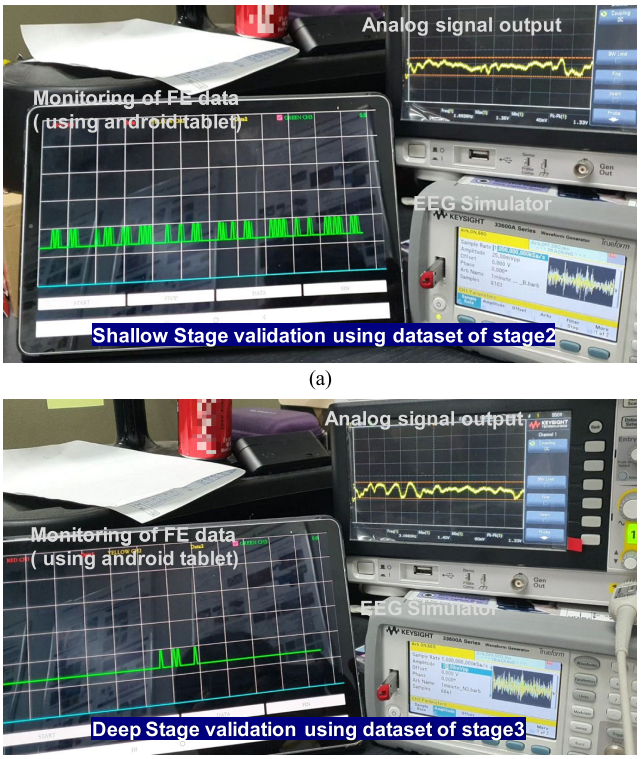

FIGURE 9. Functional test by sleep-stage dataset: (a) shallow stage (SS) and (b) deep stage (DS).

TABLE 3. Confusion matrices for sleep stage classification with multibiosignal interface using dataset.

dataset1	Shallow Sleep	Deep Sleep
Shallow Sleep	82	12
Deep Sleep	18	88

dataset2	Shallow Sleep	Deep Sleep
Shallow Sleep	78	11
Deep Sleep	22	89

	dataset1	dataset2
Sensitivity,%	87	87
Specificity,%	83	80
Accuracy,%	85	83.5
Cohen's k	0.7	0.67

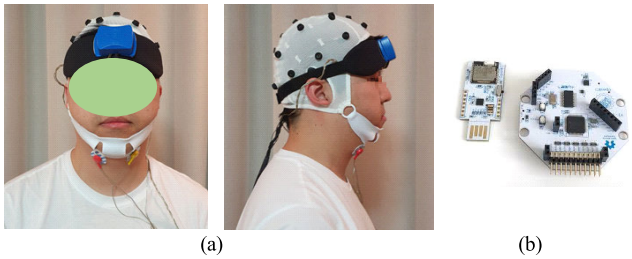

FIGURE 10. Comparison of proposed work and OpenBCI device. (a) comparison test environment, and (b) OpenBCI module.

analysis integrated interface with the sleep-EDF datasets are shown in Table 3.

The comparison experiment was performed with the commercial product of the OpenBCI which provide high-resolution EEG interface through the ADS1299 chip of the

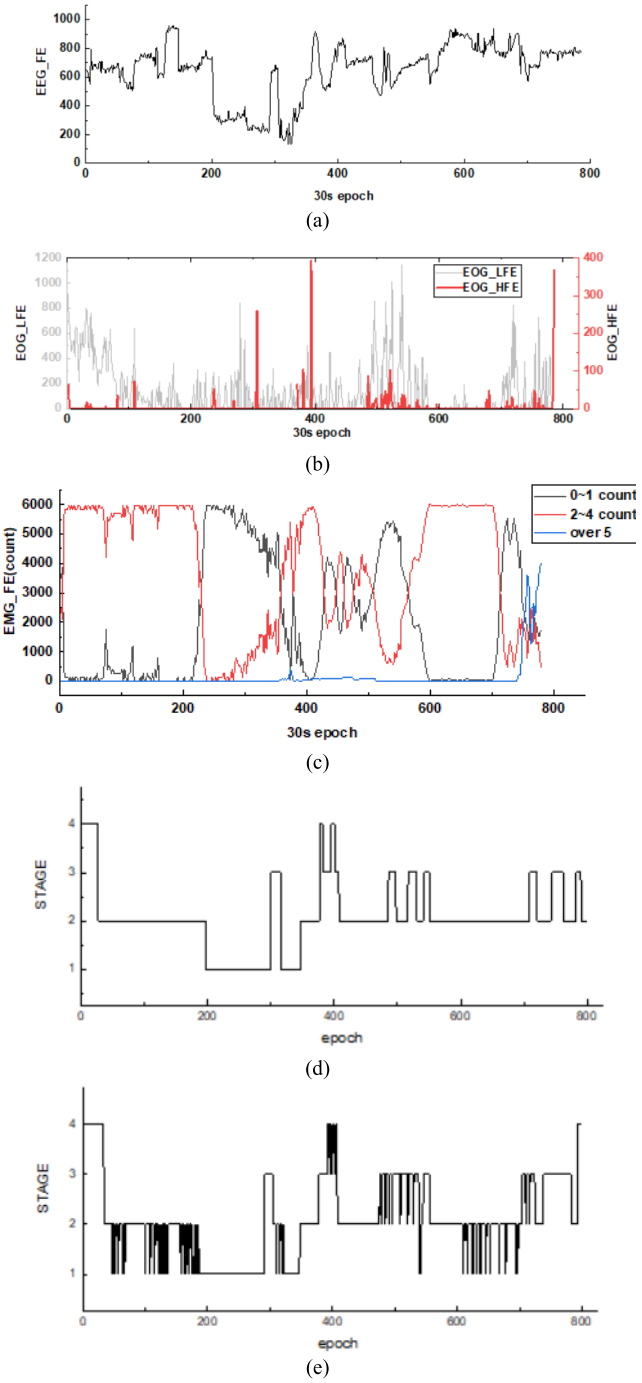

FIGURE 11. Measurements of feature extraction stage outputs and sleep stage classification for 6 hours 40 minutes: (a) feature extraction of EEG, (b) feature extraction of EOG, (c) feature extraction of EMG, (d) hypnogram by proposed device, and (e) hypnogram by OpenBCI using SVM classifier.

Texas Instrument. It is a kind of proven open-source device that has been utilized in various EEG researches [29]–[33]. As shown in Fig. 10, the OpenBCI product was worn on the upper part of the head, and the proposed prototype of the Smart headband was worn on the front forehead. Two frontal electrodes of F4 and F3 in the 10-20 EEG system [4] was utilized for the reference measurement with the OpenBCI,

TABLE 4. Performance summary and comparison of wearable devices for sleep-stage classification.

	This work	[5]	[10]	[34]	[35]
Wearable types	Headband	Portable type	Headband	Wrist band and pillow type	Wrist band
Target signal	1ch EEG, 2ch EOG, 1ch EMG	EEG, EOG, EMG, EKG, airflow	4ch EEG	Heartrate Body-movement	Actigraphy
ADC resolution	16bit	12bit	24bit	10bit	-
Power consumtion	70.9mW (Module 70mW ROIC 0.9mW)	83mW	225mW	Use power source	30mW
Sleep stages	Wake, Shallow(N1+N2), Deep(N3),REM	Wake,N1,N2, N3,REM	Wake,N1,N2, N3,REM	N1,N2,N3, REM	Wake,N1,N2, N3,REM
Classifier	Decision tree	- (clinician scoring)	SVM	Fuzzy inference and finite-state machine	RNN
Performance	74%	85.4%	76.7%	83%	85.9%
Analysis interface	**Built in self analysis**	Matlab based PC interface	Matlab based PC interface	Server	Matlab based PC interface
Hardware implementation	**ASIC**	Discrete IC	Discrete IC	Discrete IC	Discrete IC

whose sleep classification was performed by using the SVM classifier from the MATLAB. Fig. 11 shows measurement results of the comparison experiment for 6 hours 40 minutes on a 32-year-old adult male. Fig. 11(a) shows the feature extraction data of the EEG for one epoch of about the 30s, where the sleep-stage transition from the SS to the DS occurs at about 200-epoch point. Fig. 11(b) shows the feature extraction data of the EOG, where the gray line is EOG_LFE to count low-level peaks and the red line is EOG_HFE to count high-level peaks. These EOG feature extraction signals are used to differentiate between the REM and the Wake depending on their counted values as seen in the rule-based decision tree algorithm. For the EMG feature extraction, the counting speed of the EMG signal level detector is adjusted to give only 0 to 10 values. The counting outputs are grouped so that the REM, the NREM, and the Wake corresponds to $0 \sim 1$, $2 \sim 4$, and over 5 respectively.. These values are also counted for each epoch and are shown as in Fig. 11(c). The epoch of the initial EMG_FE is mostly occupied by 2 to 4 red lines. However, it is reversed around the 200-epoch point where the EEG_FE gave the transition to the DS. Fig. 11(d) and Fig. 11(e) show measured sleep-stage classification results with the hypnogram for the performance comparison, where their classification correlation of 74% was achieved. Table 4 summarized these measurement results together with the performance comparison with other recent healthcare device works.

V. CONCLUSION

This paper presented a wearable multi-biosignal integrated analysis interface embedding the direct sleep-stage detection function. Its ROIC was designed and fabricated to provide four multi-biosignal readout channels, which integrated together a proposed feature extraction circuit to utilize the EEG TEO operator, the EMG level detector, and the EOG peak detector. For system-level feasibility, a headband-style wearable module prototype was manufactured and functionally verified to provide both wireless multi-biosignal monitoring and direct sleep-stage detection. It would release heavy post-processing burdens in conventional sleep-stage analyses and facilitate stand-alone wearable devices with self-analysis capability of sleep-stage classification.

REFERENCES

[1] L. Xie, H. Kang, Q. Xu, M. J. Chen, Y. Liao, M. Thiyagarajan, J. O'Donnell, D. J. Christensen, C. Nicholson, J. J. Iliff, T. Takano, R. Deane, and M. Nedergaard, "Sleep drives metabolite clearance from the adult brain," *Science*, vol. 342, no. 6156, pp. 373–377, Oct. 2013.

[2] S. J. McCarter, E. K. St. Louis, C. L. Boswell, L. G. Dueffert, N. Slocumb, B. F. Boeve, M. H. Silber, E. J. Olson, T. I. Morgenthaler, and M. Tippmann-Peikert, "Factors associated with injury in REM sleep behavior disorder," *Sleep Med.*, vol. 15, no. 11, pp. 1332–1338, 2014.

[3] J. E. Ferrie, M. Kumari, P. Salo, A. Singh-Manoux, and M. Kivimaki, "Sleep epidemiology–A rapidly growing field," *Int. J. Epidemiol.*, vol. 40, no. 6, pp. 1431–1437, Dec. 2011.

[4] C. Iber, S. Ancoli-Israel, A. Chesson, SF. Quan, *The AASM Manual for the Scoring of Sleep and Associated Events: Rules, Terminology, and Technical Specification*, 1st ed. Westchester, IL, USA: American Academy of Sleep Medicine, 2007.

[5] G. Matar, J.-M. Lina, J. Carrier, and G. Kaddoum, "Unobtrusive sleep monitoring using cardiac, breathing and movements activities: An exhaustive review," *IEEE Access*, vol. 6, pp. 45129–45152, 2018.

[6] C.-T. Lin, M. Prasad, C.-H. Chung, D. Puthal, H. El-Sayed, S. Sankar, Y.-K. Wang, J. Singh, and A. K. Sangaiah, "IoT-based wireless polysomnography intelligent system for sleep monitoring," *IEEE Access*, vol. 6, pp. 405–414, 2017.

[7] E. Dafna, A. Tarasiuk, and Y. Zigel, "Sleep staging using nocturnal sound analysis," *Sci. Rep.*, vol. 8, p. 13474, Sep. 2018.

[8] D. J. Levendowski, L. Ferini-Strambi, C. Gamaldo, M. Cetel, R. Rosenberg, and P. R. Westbrook, "The accuracy, Night-to-Night variability, and stability of frontopolar sleep electroencephalography biomarkers," *J. Clin. Sleep Med.*, vol. 13, no. 6, pp. 791–803, Jun. 2017.

[9] E. Fino, "(Not so) Smart sleep tracking through the phone: Findings from a polysomnography study testing the reliability of four sleep applications," *J. Sleep Res.*, vol. 29, no. 1, 2019, Art. no. e12935, doi: 10.1111/jsr.12935.

[10] C.-T. Lin, C.-H. Chuang, Z. Cao, A. K. Singh, C.-S. Hung, Y.-H. Yu, M. Nascimben, Y.-T. Liu, J.-T. King, T.-P. Su, and S.-J. Wang, "Forehead EEG in support of future feasible personal healthcare solutions: Sleep management, headache prevention, and depression treatment," *IEEE Access*, vol. 5, pp. 10612–10621, 2017.

[11] G. Surrel, A. Aminifar, F. Rincon, S. Murali, and D. Atienza, "Online obstructive sleep apnea detection on medical wearable sensors," *IEEE Trans. Biomed. Circuits Syst.*, vol. 12, no. 4, pp. 762–773, Aug. 2018.

[12] Y. J. Jeon and S. J. Kang, "Wearable sleepcare kit: Analysis and prevention of sleep apnea symptoms in real-time," *IEEE Access*, vol. 7, pp. 60634–60649, 2019.

[13] J. Virkkala, J. Hasan, A. Värri, S.-L. Himanen, and K. Müller, "Automatic sleep stage classification using two-channel electro-oculography," *J. Neurosci. Methods*, vol. 166, no. 1, pp. 109–115, Oct. 2007.

[14] A. Patanaik, J. L. Ong, J. J. Gooley, S. Ancoli-Israel, and M. W. L. Chee, "An end-to-end framework for real-time automatic sleep stage classification," *Sleep*, vol. 41, no. 5, Mar. 2018, Art. no. zsy041.

[15] A. Malafeev, D. Laptev, S. Bauer, X. Omlin, A. Wierzbicka, A. Wichniak, W. Jernajczyk, R. Riener, J. Buhmann, and P. Achermann, "Automatic human sleep stage scoring using deep neural networks," *Frontiers Neurosci.*, vol. 12, p. 781, Nov. 2018, doi: 10.3389/fnins.2018.00781.

[16] S.-F. Liang, C.-E. Kuo, Y.-H. Hu, and Y.-S. Cheng, "A rule-based automatic sleep staging method," *J. Neurosci. Methods*, vol. 205, no. 1, pp. 169–176, Mar. 2012.

[17] S. Roomkham, D. Lovell, J. Cheung, and D. Perrin, "Promises and challenges in the use of consumer-grade devices for sleep monitoring," *IEEE Rev. Biomed. Eng.*, vol. 11, pp. 53–67, 2018.

[18] H. Jasper, "Report of the committee on methods of clinical examination in electroencephalography," *Electroencephalogr. Clin. Neurophysiol.*, vol. 10, no. 2, pp. 370–371, May 1958.

[19] B. P. Lucey, J. S. Mcleland, C. D. Toedebusch, J. Boyd, J. C. Morris, E. C. Landsness, K. Yamada, and D. M. Holtzman, "Comparison of a single-channel EEG sleep study to polysomnography," *J. Sleep Res.*, vol. 25, no. 6, pp. 625–635, Jun. 2016.

[20] S.-F. Liang, C.-E. Kuo, Y.-H. Hu, Y.-H. Pan, and Y.-H. Wang, "Automatic stage scoring of single-channel sleep EEG by using multiscale entropy and autoregressive models," *IEEE Trans. Instrum. Meas.*, vol. 61, no. 6, pp. 1649–1657, Jun. 2012.

[21] K. Cervena, F. Espa, L. Perogamvros, S. Perrig, H. Merica, and V. Ibanez, "Spectral analysis of the sleep onset period in primary insomnia," *Clin. Neurophysiol.*, vol. 125, no. 5, pp. 979–987, May 2014.

[22] J. F. Kaiser, "Some useful properties of Teager's energy operators," in *Proc. IEEE Int. Conf. Acoust. Speech Signal Process.*, vol. 3, Apr. 1993, pp. 149–152.

[23] W. Godycki, R. Dokania, X. Wang, and A. Apsel, "A high-speed, on-chip implementation of teager kaiser operator for in-band interference rejection," in *Proc. IEEE Asian Solid-State Circuits Conf.*, Nov. 2010, pp. 149–152.

[24] S. Iranmanesh and E. Rodriguez-Villegas, "An ultralow-power sleep spindle detection system on chip," *IEEE Trans. Biomed. Circuits Syst.*, vol. 11, no. 4, pp. 858–866, Aug. 2017.

[25] M. Neuman, "Biopotential amplifiers," in *Medical Instrumentation: Application and Design*, J. Webster, Ed., 4th ed. Hoboken, NJ, USA: Wiley, 2009, pp. 277–278.

[26] R. Ferri, M. Manconi, G. Plazzi, O. Bruni, S. Vandi, P. Montagna, L. Ferini-Strambi, and M. Zucconi, "A quantitative statistical analysis of the submentalis muscle EMG amplitude during sleep in normal controls and patients with REM sleep behavior disorder," *J. Sleep Res.*, vol. 17, no. 1, pp. 89–100, Mar. 2008.

[27] O. Yildirim, U. B. Baloglu, U. R. Acharya, "A deep learning model for automated sleep stages classification using psg signals," *Int. J. Environ. Res. Public Health*, vol. 16, no. 4, p. 599, Feb. 2019.

[28] PhysioNet. *The Sleep-Edf Database Expanded*. Accessed: Dec. 19, 2019. [Online]. Available: https://www.physionet.org/content/sleep-edfx/1.0.0/

[29] J. M. Qiu, M. A. Casey, and S. G. Diamond, "Assessing feedback response with a wearable electroencephalography system," *Frontiers Hum. Neurosci.*, vol. 13, p. 258, Jul. 2019, doi: 10.3389/fnhum.2019.00258.

[30] P. Lakhan, N. Banluesombatkul, V. Changniam, R. Dhithijaiyratn, P. Leelaarporn, E. Boonchieng, S. Hompoonsup, and T. Wilaiprasitporn, "Consumer grade brain sensing for emotion recognition," *IEEE Sensors J.*, vol. 19, no. 21, pp. 9896–9907, Nov. 2019.

[31] L. Jiang, A. Stocco, D. M. Losey, J. A. Abernethy, C. S. Prat, and R. P. N. Rao, "BrainNet: A multi-person Brain-to-Brain interface for direct collaboration between brains," *Sci. Rep.*, vol. 9, no. 1, p. 6115, Apr. 2019, doi: 10.1038/s41598-019-41895-7.

[32] R. Terracciano, A. Sanginario, S. Barbero, D. Putignano, L. Canavese, and D. Demarchi, "Pattern-reversal visual evoked potential on smart glasses," *IEEE J. Biomed. Health Inform.*, vol. 24, no. 1, pp. 226–234, Jan. 2020, doi: 10.1109/JBHi.2019.2899774.

[33] O. Valentin, M. Ducharme, G. Crétot-Richert, H. Monsarrat-Chanon, G. Viallet, A. Delnavaz, and J. Voix, "Validation and benchmarking of a wearable EEG acquisition platform for real-world applications," *IEEE Trans. Biomed. Circuits Syst.*, vol. 13, no. 1, pp. 103–111, Feb. 2019.

[34] J. Ye, Y. Lin, Z. Li, J. Lee, A.-A. Abdulrahman, and M. Jin, "A non-invasive sleep analysis approach based on a fuzzy inference system and a finite state machine," *IEEE Access*, vol. 7, pp. 2664–2676, 2018.

[35] R. Dick, T. Penzel, I. Fietze, M. Partinen, H. Hein, and J. Schulz, "AASM standards of practice compliant validation of actigraphic sleep analysis from SOMNOwatch versus polysomnographic sleep diagnostics shows high conformity also among subjects with sleep disordered breathing," *Physiol. Meas.*, vol. 31, no. 12, pp. 1623–1633, 2010.

SUNG-WOO KIM received the B.S. degree in electronic engineering from Dankook University, Yongin, South Korea, in 2012. He is currently pursuing the Ph.D. degree in electrical engineering with the Ulsan National Institute of Science and Technology, Ulsan, South Korea. His research interest includes CMOS readout circuits for bio/environmental sensor interface circuit and systems.

KWANGMUK LEE received the B.S. degree in electrical and computer engineering from the Ulsan National Institute of Science and Technology, Ulsan, South Korea, in 2015, where he is currently pursuing the Ph.D. degree in electrical engineering. His research interest includes healthcare system design, in particular CMOS biomedical circuits.

JUNYEONG YEOM received the B.S. degree in electrical and computer engineering from the Ulsan National Institute of Science and Technology, Ulsan, South Korea, in 2018. He is currently pursuing the joint M.S.-Ph.D. degrees in electrical engineering. His research interest includes integrated circuits, in particular CMOS biomedical circuits.

TAE-HOON LEE received the B.S., master's, and Ph.D. degrees in medicine from Dong-A University, Busan, South Korea, in 2001, 2004, and 2011, respectively. Since 2007, he has been a Faculty Member with the Department of Otorhinolaryngology-Head and Neck Surgery, Ulsan University Hospital, Ulsan, South Korea. From 2017 to 2018, he was a Visiting Research Scholar with the Stanford University School of Medicine. His research interest includes sleep and clinical application of 3D printing.

DON-HAN KIM received the Ph.D. degree in design from Tsukuba University, Tsukuba, Japan, in 1998. He has been a Professor with the University of Ulsan. In 2012, he founded Nextcore Company Ltd., as the Chief Executive Officer, Ulsan, South Korea, which is a 3D printing-based healthcare specialty development company. His research interests include emotion measurement with evaluation, human interface design, and intelligent emotional search systems.

JAE JOON KIM (Senior Member, IEEE) received the B.S. degree in electronic engineering from Hanyang University, Seoul, South Korea, in 1996, and the M.S. and Ph.D. degrees in electrical engineering from the Korea Advanced Institute of Science and Technology, Daejeon, South Korea, in 1998 and 2003, respectively. From 2000 to 2001, he was with Berkana Wireless, Inc., San Jose, CA, USA (now merged into Qualcomm, Inc.), where he was involved in designing wireless transceivers. From 2003 to 2005, he was with Hynix Semiconductor, Seoul, where he was involved in wireless transceivers and smart-card controllers. From 2005 to 2011, he was the Deputy Director of the Ministry of Information and Communications, Korean Government, and the Ministry of Trade, Industry and Energy. From 2009 to 2011, he was a Research Engineer II with the Georgia Institute of Technology, Atlanta, GA, USA. Since 2011, he has been an Associate Professor with the Ulsan National Institute of Science and Technology, Ulsan, South Korea. His research interests include integrated circuits and systems for smart sensor interfaces, wearable healthcare devices, consumer electronics, automotive electronics, and wireless transceivers.